Laplace transform integration of the shallow water equations. Part 2: Semi-Lagrangian formulation and orographic resonance

Colm Clancy* and Peter Lynch

School of Mathematical Sciences, UCD, Belfield, Dublin 4, Ireland

*Correspondence to: School of Mathematical Sciences, UCD, Belfield, Dublin 4, Ireland. E-mail: Colm.Clancy@ucd.ie

In this paper we combine the Laplace transform (LT) scheme with a semi-Lagrangian advection scheme, and implement it in a shallow water model. It is compared to a reference model using the semi-implicit (SI) scheme, with both Eulerian and Lagrangian advection. We show that the LT scheme is accurate and computationally competitive with these reference schemes. We also show, both analytically and numerically, that the LT scheme is free from the problem of orographic resonance that is found with semi-implicit schemes. Copyright © 0000 Royal Meteorological Society

Key Words: Numerical weather prediction; Time integration; Filtering

Received . . .

Citation: . . .

1. Introduction

In this paper a semi-Lagrangian Laplace transform (SLLT) shallow water model is developed. In Clancy and Lynch (2011), referenced below as Part 1, we introduced the Laplace transform (LT) scheme for time integration and implemented it in a model using Eulerian advection. The scheme was shown to have advantages when compared to a reference semi-implicit (SI) scheme. In particular, it was able to simulate Kelvin waves with greater accuracy.

The size of the timestep used with an Eulerian advection scheme is limited by constraints of stability rather than accuracy. By combining the semi-implicit averaging with a semi-Lagrangian treatment of advection, Robert (1981, 1982) was able to perform stable and accurate integrations with even longer timesteps. Bates and McDonald (1982) showed that there was no CFL restriction with the semi-Lagrangian advection scheme, and were the first to implement it in an operational forecast model. Further details on the development of semi-Lagrangian methods may be found in the review of Staniforth and Côté (1991).

A combined semi-Lagrangian and LT scheme for a shallow water model is formulated in §2. We use a spectral method for the spatial discretisation and test the model against reference Eulerian and semi-Lagrangian semi-implicit versions. The stability and accuracy of the scheme are analysed. We use a two time level discretisation for the SLLT scheme. Two time level semi-Lagrangian schemes offer a doubling of efficiency compared to three time level versions (Temperton et al. 2001). In §3 the SLLT scheme will be evaluated using the test cases of Willimason et al. (1992). A number of variations of the SLLT discretisation are discussed. Its symmetry and stability properties are also examined.

We explore the problem of orographic resonance in §4. This is a spurious noise that results from the coupling of the semi-implicit and semi-Lagrangian schemes at high CFL numbers. We investigate the problem analytically and show that, in a simple linear model, the semi-Lagrangian Laplace transform scheme is free from this problem. We confirm that this result holds for the fully nonlinear shallow water equations by numerical tests. Finally, §5 contains a summary of the main results.

2. Shallow water model

Two semi-Lagrangian models were developed; one using a semi-implicit discretisation and the other with the LT method. These are based on a spectral transform shallow water model called *SWEmodel*, written in Matlab. This model is described in Drake and Guo (2001), with the spherical harmonic transform routines documented in Drake et al. (2008). The original code included an Eulerian shallow water model, which we will also use as a reference.

2.1. Semi-Lagrangian semi-implicit: SLSI

The shallow water equations are written in the form

$$\begin{aligned}\frac{\mathrm{d}\zeta}{\mathrm{d}t} + f\delta + \beta v &= N_\zeta \\ \frac{\mathrm{d}\delta}{\mathrm{d}t} - f\zeta + \beta u + \nabla^2\Phi &= N_\delta \\ \frac{\mathrm{d}\Phi}{\mathrm{d}t} - \frac{\mathrm{d}\Phi_s}{\mathrm{d}t} + \bar{\Phi}\delta &= N_\Phi \end{aligned} \tag{1}$$

where ζ is the relative vorticity, δ is the horizontal divergence and $\beta = \frac{1}{a}\frac{\partial f}{\partial \phi}$. The constant reference geopotential is $\bar{\Phi}$, with Φ representing the deviation of the geopotential height from this reference. The surface geopotential is Φ_s. The nonlinear terms are

$$\begin{aligned} N_\zeta &\equiv -\zeta\delta \\ N_\delta &\equiv \zeta^2 - \nabla^2\left(\frac{\mathbf{v}.\mathbf{v}}{2}\right) + \frac{u}{\cos\phi}\left(\nabla^2(u\cos\phi) - \frac{2\sin\phi}{a}\zeta\right) \\ &\quad + \frac{v}{\cos\phi}\left(\nabla^2(v\cos\phi) + \frac{2\sin\phi}{a}\delta\right) \\ N_\Phi &\equiv -(\Phi - \Phi_s)\delta \end{aligned}$$

For the semi-Lagrangian semi-implicit (SLSI) model, a two time level discretisation is used. All linear terms are averaged in time, including the Coriolis terms (Temperton and Staniforth, 1987; Côté and Staniforth, 1988). The discretised system can then be written as

$$\begin{aligned} \zeta_A^{n+1} + \frac{\Delta t}{2} f\delta_A^{n+1} + \frac{\Delta t}{2}\beta v_A^{n+1} &= R_\zeta \\ \delta_A^{n+1} - \frac{\Delta t}{2} f\zeta_A^{n+1} + \frac{\Delta t}{2}\beta u_A^{n+1} + \frac{\Delta t}{2}\{\nabla^2\Phi\}_A^{n+1} &= R_\delta \\ \Phi_A^{n+1} + \frac{\Delta t}{2}\bar{\Phi}\delta_A^{n+1} &= R_\Phi \end{aligned} \tag{2}$$

with

$$\begin{aligned} R_\zeta &= \left\{\zeta - \frac{\Delta t}{2} f\delta - \frac{\Delta t}{2}\beta v\right\}_D^n + \Delta t\{N_\zeta\}_M^{n+\frac{1}{2}} \\ R_\delta &= \left\{\delta + \frac{\Delta t}{2} f\zeta - \frac{\Delta t}{2}\beta u - \frac{\Delta t}{2}\nabla^2\Phi\right\}_D^n + \Delta t\{N_\delta\}_M^{n+\frac{1}{2}} \\ R_\Phi &= \left\{\Phi - \Phi_s - \frac{\Delta t}{2}\bar{\Phi}\delta\right\}_D^n + (\Phi_s)_A + \{N_\Phi\}_M^{n+\frac{1}{2}} \end{aligned}$$

Here $\{\ \}_A^{n+1}$ refers to an arrival value at a regular gridpoint at time $(n+1)\Delta t$ with the corresponding departure value $\{\ \}_D^n$ at time $n\,\Delta t$. Values at the trajectory's midpoint are denoted $\{\ \}_M^{n+\frac{1}{2}}$.

The departure points are computed using the method outlined in Ritchie and Beaudoin (1994). For this iterative technique, an initial guess of the midpoint wind $\mathbf{v}_M^{n+\frac{1}{2}}$ is obtained with the simple two-term extrapolation

$$\left(\mathbf{v}_M^{n+\frac{1}{2}}\right)^{(0)} = \mathbf{v}_A^{n+\frac{1}{2}} = \tfrac{3}{2}\mathbf{v}_A^n - \tfrac{1}{2}\mathbf{v}_A^{n-1}$$

Other possibilities are discussed in Temperton and Staniforth (1987). Three iterations were used for this and at each step new values for $\mathbf{v}_M^{n+\frac{1}{2}}$ were computed with bilinear interpolation.

When interpolating model fields to departure or midpoints, bicubic interpolation was used. The nonlinear terms are first extrapolated in time using

$$N_A^{n+\frac{1}{2}} = \tfrac{3}{2}N_A^n - \tfrac{1}{2}N_A^{n-1}$$

before being interpolated to the midpoint values $N_M^{n+\frac{1}{2}}$. A discussion of various interpolation options is given in the review paper of Staniforth and Côté (1991).

The system is solved using a spectral method. Each field is expanded in terms of spherical harmonics, e.g.

$$\zeta = \sum_{\ell=0}^{L}\sum_{m=-\ell}^{\ell}\zeta_\ell^m\, Y_\ell^m(\lambda,\mu)$$

where $Y_\ell^m(\lambda,\mu) = e^{i\,m\,\lambda}\,P_\ell^m(\lambda,\mu)$ and $\mu = \sin\phi$. Orthogonality of the spherical harmonics is used to isolate individual spectral coefficients. Following Côté and Staniforth (1988), and defining $\alpha = \Omega\Delta t$ and $\varepsilon_\ell^m = \sqrt{\frac{\ell^2-m^2}{4\ell^2-1}}$, we get

$$\begin{aligned} A_\ell^m\,\zeta_\ell^m + B_\ell^m\,\delta_{\ell-1}^m + C_\ell^m\,\delta_{\ell+1}^m &= [R_\zeta]_\ell^m \\ A_\ell^m\,\delta_\ell^m - B_\ell^m\,\zeta_{\ell-1}^m - C_\ell^m\,\zeta_{\ell+1}^m & \\ -\frac{\Delta t}{2}\frac{\ell(\ell+1)}{a^2}\Phi_\ell^m &= [R_\delta]_\ell^m \\ \Phi_\ell^m + \frac{\Delta t}{2}\bar{\Phi}\delta_\ell^m &= [R_\Phi]_\ell^m \end{aligned} \tag{3}$$

with

$$\begin{aligned} A_\ell^m &= 1 - \frac{im\alpha}{\ell(\ell+1)}\ , \quad B_\ell^m = \frac{\alpha(\ell+1)}{\ell}\varepsilon_\ell^m \\ C_\ell^m &= \frac{\alpha\ell}{\ell+1}\varepsilon_{\ell+1}^m \end{aligned}$$

The spectral system can be shown to decouple to

$$\begin{aligned} &L_\ell^m\,\delta_{\ell-2}^m + M_\ell^m\,\delta_\ell^m + U_\ell^m\,\delta_{\ell+2}^m = [R_\delta]_\ell^m + \frac{\Delta t}{2}\frac{\ell\,(\ell+1)}{a^2}\,[R_\Phi]_\ell^m \\ &+ \frac{\alpha\,(\ell^2-1)\,\varepsilon_\ell^m}{\ell\,(\ell-1) - i\,m\,\alpha}\,[R_\zeta]_{\ell-1}^m + \frac{\alpha\,\ell\,(\ell+2)\,\varepsilon_{\ell+1}^m}{(\ell+1)(\ell+2) - i\,m\,\alpha}\,[R_\zeta]_{\ell+1}^m \\ &\Phi_\ell^m = [R_\Phi]_\ell^m - \frac{\Delta t}{2}\,\bar{\Phi}\,\delta_\ell^m \\ &\zeta_\ell^m = \frac{\ell\,(\ell+1)\,[R_\zeta]_\ell^m - \alpha\,(\ell+1)^2\,\varepsilon_\ell^m\,\delta_{\ell-1}^m - \alpha\,\ell^2\,\varepsilon_{\ell+1}^m\,\delta_{\ell+1}^m}{\ell\,(\ell+1) - i\,m\,\alpha} \end{aligned} \tag{4}$$

where

$$\begin{aligned} L_\ell^m &= \frac{\alpha^2\,(\ell^2+\ell)\,\varepsilon_{\ell-1}^m\,\varepsilon_\ell^m}{\ell^2 - \ell - i\,m\,\alpha} \\ M_\ell^m &= 1 - \frac{i\,m\,\alpha}{\ell\,(\ell+1)} + \left(\frac{\Delta t}{2}\right)^2\bar{\Phi}\frac{\ell\,(\ell+1)}{a^2} + \\ &\frac{(\alpha\,\varepsilon_\ell^m)^2\,(\ell-1)^2(\ell+1)}{\ell^2\,(\ell-1) - i\,m\,\ell\,\alpha} + \frac{(\alpha\,\varepsilon_{\ell+1}^m)^2\,\ell\,(\ell+2)^2}{(\ell+1)^2\,(\ell+2) - i\,m\,\alpha\,(\ell+1)} \\ U_\ell^m &= \frac{\alpha^2\,(\ell^2+\ell)\,\varepsilon_{\ell+1}^m\,\varepsilon_{\ell+2}^m}{(\ell+1)\,(\ell+2) - i\,m\,\alpha} \end{aligned}$$

If odd and even values of ℓ are considered separately for every m, the system yields two tridiagonal matrix systems for the coefficients δ_ℓ^m which can be efficiently solved (Durran, 1999).

2.2. *Semi-Lagrangian Laplace transform: SLLT*

We consider a general evolution equation in Lagrangian form

$$\frac{\mathrm{d}X}{\mathrm{d}t} + LX = N(X) \tag{5}$$

The total derivative $\mathrm{d}X/\mathrm{d}t$ represents the change along the trajectory of the fluid parcel. In the LT scheme of Lynch (1991), the advection terms are separated when formulating a Lagrangian approach and the Eulerian time derivative is then transformed. In the present scheme we take the Laplace transform *along the time-dependent trajectory* of a parcel arriving at a gridpoint A at time level $(n+1)$. Formally, we are integrating along the trajectory contour $\mathcal{T}$ so that

$$\widehat{X} \equiv \int_{\mathcal{T}} e^{-s\,\tau}\, X \,\mathrm{d}\tau \tag{6}$$

With a two time level approach, this trajectory starts at time n at some departure point D, not necessarily coinciding with a gridpoint. This is the 'initial value' when taking the transform of a Lagrangian derivative. The transform of the prognostic equation (5) can then be written

$$s\,\widehat{X} - X_D^n + L\widehat{X} = \frac{1}{s}\, N_M^{n+\frac{1}{2}} \tag{7}$$

Here the nonlinear terms have been evaluated at the midpoint M of the trajectory and at time level $n+\frac{1}{2}$. This constant value is then transformed.

We apply this to the system (1), yielding

$$\begin{aligned}
s\,\widehat{\zeta} - \zeta_D^n + \widehat{f\delta} + \widehat{\beta v} &= \frac{1}{s}\{N_\zeta\}_M^{n+\frac{1}{2}} \\
s\,\widehat{\delta} - \delta_D^n - \widehat{f\zeta} + \widehat{\beta u} + \widehat{\nabla^2\Phi} &= \frac{1}{s}\{N_\delta\}_M^{n+\frac{1}{2}} \\
s\widehat{\Phi} - \Phi_D^n - \frac{\widehat{\mathrm{d}\Phi_s}}{\mathrm{d}t} + \bar{\Phi}\widehat{\delta} &= \frac{1}{s}\{N_\Phi\}_M^{n+\frac{1}{2}}
\end{aligned}$$

The Coriolis terms need special consideration. Though constant in time, both f and β vary along a trajectory. This means that transforms of products such as $\widehat{f\delta}$ cannot be easily separated and make the system very difficult to decouple.

One approach to overcome this is to assume that the changes in f and β along a trajectory are negligible, which allows us to write

$$\begin{aligned}
\widehat{f\delta} &\to f_A\,\widehat{\delta}\,, \quad \widehat{f\zeta} \to f_A\,\widehat{\zeta} \\
\widehat{\beta u} &\to \beta_A\,\widehat{u}\,, \quad \widehat{\beta v} \to \beta_A\,\widehat{v}
\end{aligned}$$

These are used for the SLLT model in this work. Alternatives were explored, but these approximations were found to give the best results (Clancy, 2010). The transform of the orography $\widehat{\frac{\mathrm{d}\Phi_s}{\mathrm{d}t}}$ also requires care. Like the Coriolis terms, this is time-independent but varies along a trajectory. If we assume the change to be small and treat it as 'constant' at its arrival value, the orographic derivative term transforms to

$$\begin{aligned}
\frac{\widehat{\mathrm{d}\Phi_s}}{\mathrm{d}t} &= s\,\widehat{\Phi_s} - (\Phi_s)_D^n = s\left(\frac{(\Phi_s)_A^{n+1}}{s}\right) - (\Phi_s)_D^n \\
&= (\Phi_s)_A^{n+1} - (\Phi_s)_D^n
\end{aligned}$$

An alternative would be first to discretise the derivative as

$$\frac{\mathrm{d}\Phi_s}{\mathrm{d}t} = \frac{(\Phi_s)_A^{n+1} - (\Phi_s)_D^n}{\Delta t}$$

The terms on the right are now all constants and so we can easily take the LT to get

$$\frac{\widehat{\mathrm{d}\Phi_s}}{\mathrm{d}t} = \frac{(\Phi_s)_A^{n+1} - (\Phi_s)_D^n}{s\,\Delta t}$$

Both methods were tested: the second was found to give superior results in simulations and so was implemented in the main SLLT code.

With the above approximations, the system to be solved is now

$$\begin{aligned}
s\widehat{\zeta} + f\,\widehat{\delta} + \beta\,\widehat{v} &= R_\zeta \\
s\widehat{\delta} - f\,\widehat{\zeta} + \beta\,\widehat{u} + \nabla^2\widehat{\Phi} &= R_\delta \\
s\widehat{\Phi} + \bar{\Phi}\,\widehat{\delta} &= R_\Phi
\end{aligned} \tag{8}$$

where we note that $\widehat{\nabla^2\Phi} = \nabla^2\widehat{\Phi}$. The right-hand terms are

$$\begin{aligned}
R_\zeta &= \zeta_D^n + \frac{1}{s}\{N_\zeta\}_M^{n+\frac{1}{2}} \\
R_\delta &= \delta_D^n + \frac{1}{s}\{N_\delta\}_M^{n+\frac{1}{2}} \\
R_\Phi &= \Phi_D^n + \frac{(\Phi_s)_A - (\Phi_s)_D}{s\,\Delta t} + \frac{1}{s}\{N_\Phi\}_M^{n+\frac{1}{2}}
\end{aligned}$$

Each transformed variable is a function of space and the complex variable s and so they can be expanded in terms of spherical harmonics; for example

$$\widehat{\zeta}(s,\lambda,\mu) = \sum_\ell \sum_m \widehat{\zeta}_\ell^m(s) Y_\ell^m(\lambda,\mu)$$

Note that the spectral coefficients in this case are functions of s. The system (8) can thus be solved spectrally, in a manner similar to the SLSI scheme, for a given value of s. Using orthogonality as before, we get the following

$$\begin{aligned}
\tilde{A}_\ell^m \left(s\,\widehat{\zeta}_\ell^m\right) + \tilde{B}_\ell^m \left(s\,\widehat{\delta}_{\ell-1}^m\right) + \tilde{C}_\ell^m \left(s\,\widehat{\delta}_{\ell+1}^m\right) &= [R_\zeta]_\ell^m \\
\tilde{A}_\ell^m \left(s\,\widehat{\delta}_\ell^m\right) - \tilde{B}_\ell^m \left(s\,\widehat{\zeta}_{\ell-1}^m\right) - \tilde{C}_\ell^m \left(s\,\widehat{\zeta}_{\ell+1}^m\right) & \\
-\frac{1}{s}\frac{\ell(\ell+1)}{a^2}\left(s\,\widehat{\Phi}_\ell^m\right) &= [R_\delta]_\ell^m \\
\left(s\,\widehat{\Phi}_\ell^m\right) + \frac{1}{s}\bar{\Phi}\left(s\,\widehat{\delta}_\ell^m\right) &= [R_\Phi]_\ell^m
\end{aligned} \tag{9}$$

with

$$\begin{aligned}
\tilde{A}_\ell^m &= 1 - \frac{im}{\ell(\ell+1)}\,\frac{2\Omega}{s}\,, \quad \tilde{B}_\ell^m = \frac{(\ell+1)}{\ell}\,\frac{2\Omega}{s}\,\varepsilon_\ell^m \\
\tilde{C}_\ell^m &= \frac{\ell}{\ell+1}\,\frac{2\Omega}{s}\,\varepsilon_{\ell+1}^m
\end{aligned}$$

The above matches (3) with $1/s$ here replacing $\Delta t/2$. As in the SLSI case, this system can be decoupled to give two tridiagonal matrix systems for the $\widehat{\delta}_\ell^m$ coefficients. We can

solve these and then evaluate all the $\widehat{\Phi}_\ell^m$ and $\widehat{\zeta}_\ell^m$. Once these are known we can synthesise each of the transformed fields $\widehat{\delta}$, $\widehat{\Phi}$ and $\widehat{\zeta}$. For SLLT this must be done for each value of s on the inversion contour. We can then invert to the physical field at the new time level with the summation outlined in Part 1; for example

$$\delta = \frac{1}{N}\sum_{n=1}^{N} s_n\, \widehat{\delta}(s_n)\, e_N^{s_n \Delta t}$$

2.3. *Symmetry*

In the SLSI model, we consider the spectral coefficients of a real function which have the symmetry property

$$\delta_\ell^{-m} = (-1)^m\, \overline{\delta_\ell^m}$$

where the bar denotes the complex conjugate. As a result, we only need to solve the tridiagonal systems in (4) for $m \geq 0$. In the case of SLLT, we are dealing with the spectral coefficients of the complex Laplace transform of the fields, for example, $\widehat{\delta}_\ell^m$. The symmetry in m will not now hold and we need to solve for all m.

It is possible, however, to reduce the computational overhead of the LT method. Lynch (1991) discusses a symmetry which allows us to halve the number of points on the inversion contour. For a real function $f(t)$ with LT $\widehat{f}(s)$, it follows from the definition of the transform that

$$\widehat{f}(\overline{s}) = \overline{\widehat{f}(s)}$$

On the inversion N-gon described in Part 1, the points used in the summation satisfy $s_{N+1-n} = \overline{s_n}$ for $n = 1, \ldots, N/2$. We can then write the inversion summation as

$$\begin{aligned}
\mathfrak{L}_N^*\{\widehat{f}\} &= \frac{1}{N}\sum_{n=1}^{N/2}\left\{ s_n\, \widehat{f}(s_n)\, e_N^{s_n t} + \overline{s_n}\, \widehat{f}(\overline{s_n})\, e_N^{\overline{s_n} t}\right\} \\
&= \frac{1}{N}\sum_{n=1}^{N/2}\left\{ s_n\, \widehat{f}(s_n)\, e_N^{s_n t} + \overline{s_n\, \widehat{f}(s_n)\, e_N^{s_n t}}\right\} \\
&= \frac{2}{N}\sum_{n=1}^{N/2} \Re\left\{ s_n\, \widehat{f}(s_n)\, e_N^{s_n t}\right\} \qquad (10)
\end{aligned}$$

Thus we are able to halve the number of inversion points needed for the LT method.

2.4. *Stability*

Côté and Staniforth (1988) use a logarithmic form of the continuity equation in (1) for their two time level scheme. Their stability analysis showed that, for the non-logarithmic form used in our SLSI model, the mean geopotential must be greater than the maximum geopotential height. A stability analysis of the SLLT scheme, following the approach of Durran (1999), has been carried out. The scheme is stable under lenient restrictions on the timestep and the value of N in the inversion operator. Details are given in Clancy (2010). If these conditions are not satisfied, an amplification factor slightly larger than 1 is possible. However, no problems were encountered when running the SLLT model. The model remained stable and did not require $\bar{\Phi} \geq \Phi_{\max}$ in contrast to the SLSI model.

2.5. *Summary of method*

We now present a brief summary of the SLLT algorithm:

1. Compute the right-hand sides of (8), which contain terms interpolated to the departure and midpoints
2. Compute the spectral coefficients of these and solve the system (9) for the coefficients of the transformed prognostic variables
3. Synthesise the transformed fields from their spectral coefficients
4. Use the numerical operator in (10) to invert to the time domain to get the solutions at the new time level

The order of 3. and 4. may be reversed, with possible benefits to efficiency.

3. Testing the model

The SLSI and SLLT schemes were tested with cases 2, 5 and 6 from Williamson et al. (1992). No diffusion was used in these runs. Results were compared with the reference Eulerian model. For Case 2, of a nondivergent zonal flow with a geostrophically balanced height field, the errors for both the SLSI and SLLT schemes were very small, even with a 1 hour timestep. The errors for SLLT were about half the magnitude of those for SLSI.

For the mountain test case, Case 5, no analytic solution exists. We used the STSWM model detailed in Part 1, run at a T213 resolution with a 360 second timestep, as a reference. In the left panel of Figure 1 we plot the normalised l_∞ errors for the Eulerian, SLSI and SLLT models at T119 resolution with a 600 second timestep over a 240 hour simulation. For the SLLT runs we used $N = 8$ and $\tau_c = 6$ hours. In the right panel we present the errors for both semi-Lagrangian models at longer timesteps. Errors remain small, even at at a one hour timestep. The SLLT model in particular shows little variation with increasing timestep. It should be noted that imbalance in the initial conditions leads to rapid error growth in the initial few days of the forecasts.

For Case 6, the Rossby-Haurwitz wave, a T213 STSWM run was again used as a reference. The value for $\bar{\Phi}$ specified in Williamson et al. (1992), $\bar{\Phi} = gh_0$ with $h_0 = 8\,\mathrm{km}$, had to be changed for the SLSI forecasts to maintain stability, as discussed already. We used $\bar{\Phi} = 1.1 \times 10^5\,\mathrm{m^2 s^{-2}}$ in order to exceed the maximum height. The SLLT model ran without difficulty with the original value used by Williamson et al. (1992).

In the left panel of Figure 2 we see l_∞ errors for the various schemes, again at T119 and a timestep of 600 seconds. The right-hand panel shows errors at longer timesteps. The SLSI and SLLT models show comparable accuracy. Both significantly damp the wave when run with long timesteps; this is more severe for SLSI. The SLSI model would not run stably at a one hour timestep. The SLLT run remained stable, but was severely damped

For both Cases 5 and 6, the SLLT model was also tested using a cut-off period $\tau_c = 3$ hours. The accuracy remained comparable with the $\tau_c = 6$ simulations. It was, however, unstable for Case 6 with a one hour timestep. This is probably due to the stability criterion of the LT scheme described in Part 1. With $N = 8$ and $\tau_c = 3$, a one hour timestep violates this. We note that this criterion is a sufficient, but not necessary, condition. Case 5 ran successfully at a one hour timestep.

4. Orographic Resonance

The coupling of a semi-Lagrangian treatment of advection with a semi-implicit method for stabilising gravity waves allowed numerical forecasts to be carried out with timesteps considerably longer than required for Eulerian schemes (Robert 1981, 1982). While this technique was successful in permitting stable and efficient forecasts, a problem arose in the case of simulating flow over orography.

A simple analysis of the linearised shallow water equations shows that stationary waves produce an infinite response to orographic forcing when the mean flow equals the gravity wave speed. This physical phenomenon is unlikely to occur given the high speed of gravity waves and does not generally pose a problem for numerical simulations. However, Coiffier et al. (1987) showed that a semi-Lagrangian semi-implicit discretisation introduces a spurious resonant response at large Courant numbers. Numerical runs confirmed this analysis. As the main advantage of a SLSI scheme was the ability to run at large timesteps, this problem was a cause for concern.

A number of solutions have been proposed. Tanguay et al. (1992) show that by spatially averaging all nonlinear terms, the distortions near orography are reduced, though not fully alleviated. Rivest et al. (1994) show that this can be improved upon by off-centring the semi-implicit averaging. They examine first-order and second-order averaging and recommend the latter for better accuracy. This approach has been investigated in a number of atmospheric models; Héreil and Laprise (1996), Caya and Laprise (1999).

Ritchie and Tanguay (1996) found that the more efficient first-order off-centring is sufficient if the orographic term in the continuity equation is treated in an Eulerian rather than a Lagrangian manner. They noted, however, a truncation error evident in both approaches, which is smaller in the case of the Eulerian treatment of orography. The ECMWF model, for example, follows the approach of Ritchie and Tanguay together with the spatial averaging of Tanguay et al. (1992). The orographic contribution to the advection in the continuity equation is isolated and treated in a spatially averaged manner (Temperton et al., 2001). We note that, with the operational resolutions currently used, the model does not suffer from orographic resonance (Wedi, personal communication).

In reviewing this approach, Lindberg and Alexeev (2000) note that it has been largely successful but does not fully remove the spurious response. Li and Bates (1996) also show how off-centring can have a negative impact on large scale Rossby waves; the first-order method causes excessive damping. They find that by using a potential vorticity form of the shallow water equations, a less damaging modified off-centring is possible. In their study of a general class of off-centred schemes, Côté et al. (1995) recommend using the least amount of off-centring possible, consistant with alleviating resonance, to minimize errors.

4.1. *Linear analysis: physical response*

The shallow water equations are given in vorticity-divergence form and are linearised about a mean flow $\bar{u} = a\bar{\omega}\cos\phi$, where $\bar{\omega}$ is a constant advecting angular velocity. The Coriolis parameter f is taken to be constant. With $\frac{\mathrm{d}}{\mathrm{d}t} = \frac{\partial}{\partial t} + \bar{\omega}\frac{\partial}{\partial\lambda}$, the linearised system is

$$\begin{aligned} \frac{\mathrm{d}\zeta}{\mathrm{d}t} + f\delta &= 0 \\ \frac{\mathrm{d}\delta}{\mathrm{d}t} - f\zeta + \nabla^2\Phi &= 0 \\ \frac{\mathrm{d}\Phi}{\mathrm{d}t} + \bar{\Phi}\delta &= \frac{\mathrm{d}\Phi_s}{\mathrm{d}t} \end{aligned} \tag{11}$$

We consider solutions comprised of a single spherical harmonic as follows

$$\begin{pmatrix} \zeta \\ \delta \\ \Phi \end{pmatrix} = \begin{pmatrix} \zeta_\ell^m \\ \delta_\ell^m \\ \Phi_\ell^m \end{pmatrix} e^{i(m\lambda-\nu t)} P_\ell^m(\mu) \tag{12}$$

with $\Phi_s = (\Phi_s)_\ell^m e^{im\lambda} P_\ell^m(\mu)$. We substitute this into (11) and take $\nu = 0$ to consider orographically-forced stationary solutions. Solving then for Φ_ℓ^m we get

$$\Phi_\ell^m = \frac{(m\bar{\omega})^2 - f^2}{(m\bar{\omega})^2 - G_\ell^2} (\Phi_s)_\ell^m \tag{13}$$

where

$$G_\ell^2 \equiv f^2 + \frac{\ell(\ell+1)}{a^2}\bar{\Phi} \tag{14}$$

is the squared frequency of the gravity-inertia wave. We find a physical resonance if this frequency equals that of the mean flow.

4.2. *Linear analysis: SLSI*

Ritchie and Tanguay (1996) analyse the problem in a three time level model. Here we adapt their analysis for a two time level version. First we consider a two time level semi-Lagrangian semi-implicit (SLSI) treatment of the linearised system. The orography is treated in a Lagrangian manner and no explicit diffusion is included. Discretising (11) we get

$$\begin{aligned} &\frac{\zeta_A^{n+1} - \zeta_D^n}{\Delta t} + f\frac{\{\delta\}_A^{n+1} + \{\delta\}_D^n}{2} = 0 \\ &\frac{\delta_A^{n+1} - \delta_D^n}{\Delta t} - f\frac{\{\zeta\}_A^{n+1} + \{\zeta\}_D^n}{2} + \frac{\{\nabla^2\Phi\}_A^{n+1} + \{\nabla^2\Phi\}_D^n}{2} = 0 \\ &\frac{\Phi_A^{n+1} - \Phi_D^n}{\Delta t} + \frac{\bar{\Phi}\delta_A^{n+1} + \bar{\Phi}\delta_D^n}{2} = \frac{(\Phi_s)_A - (\Phi_s)_D}{\Delta t} \end{aligned}$$

We seek to examine the response of stationary waves to orographic forcing and so look for solutions of the form

$$\begin{pmatrix} \zeta \\ \delta \\ \Phi \\ \Phi_s \end{pmatrix} = \begin{pmatrix} \zeta_\ell^m \\ \delta_\ell^m \\ \Phi_\ell^m \\ (\Phi_s)_\ell^m \end{pmatrix} e^{im\lambda} P_\ell^m(\mu) \tag{15}$$

The effect of the discretised time derivative is, e.g.,

$$\begin{aligned} \frac{\zeta_A^{n+1} - \zeta_D^n}{\Delta t} &= \frac{\zeta_\ell^m e^{im\lambda_A} P_\ell^m - \zeta_\ell^m e^{im(\lambda_A - \bar{\omega}\Delta t)} P_\ell^m}{\Delta t} \\ &= \zeta_A^{n+1}\,\frac{2\,i}{\Delta t}\,e^{-i\,\theta}\,\sin\theta \end{aligned}$$

where $\theta \equiv \frac{m\bar{\omega}\Delta t}{2}$. Similarly,

$$\frac{\zeta_A^{n+1} + \zeta_D^n}{2} = \zeta_A^{n+1}\,e^{-i\,\theta}\cos\theta$$

We apply these results to the discretised system. Each equation is then multiplied by $\Delta t\, e^{i\theta}$ and the linear system can be solved for Φ:

$$\Phi_\ell^m = \left\{ \frac{f^2 \cos^2\theta - \left(\frac{\sin\theta}{\theta}\right)^2 (m\,\bar{\omega})^2}{G_\ell^2\, \cos^2\theta - \left(\frac{\sin\theta}{\theta}\right)^2 (m\,\bar{\omega})^2} \right\} (\Phi_s)_\ell^m \qquad (16)$$

Following Rivest et al. (1994) and Ritchie and Tanguay (1996), we consider the ratio of the numerical to the physical response and so divide the above by (13) to get

$$R_{\rm SLSI} = \frac{\left(f^2 - \left(\frac{\tan\theta}{\theta}\right)^2 (m\,\bar{\omega})^2\right)\left((m\,\bar{\omega})^2 - G_\ell^2\right)}{\left(G_\ell^2 - \left(\frac{\tan\theta}{\theta}\right)^2 (m\,\bar{\omega})^2\right)\left((m\,\bar{\omega})^2 - f^2\right)} \qquad (17)$$

We note first that $R_{\rm SLSI}$ has a zero denominator when $(m\,\bar{\omega})^2 - f^2 = 0$. As pointed out by Ritchie and Tanguay, this is not a resonance but is due to a zero value of the numerator of the physical response (13). There is, however, a spurious numerical resonance when

$$\frac{\tan\theta}{\theta} = \pm\frac{G_\ell}{m\,\bar{\omega}} \qquad (18)$$

Since G_ℓ is large, resonance occurs near the singular points of $\tan\theta$, that is,

$$\theta = \left(k + \tfrac{1}{2}\right)\pi, \text{ for } k \in \mathbb{Z} \qquad (19)$$

We present plots of $R_{\rm SLSI}$ for a T119 truncation. Following Ritchie and Tanguay we take $\ell = m$ and use the values $f = 10^{-4}\,\mathrm{s}^{-1}$ and $\bar{\Phi} = 5.6 \times 10^4\,\mathrm{m}^2\,\mathrm{s}^{-2}$. We choose the advecting wind to be 50 $\mathrm{m\,s}^{-1}$ at the equator so that $\bar{\omega} = \frac{50}{a}\,\mathrm{s}^{-1}$.

In the left panel of Figure 3 we take Δt = 600 and 3600 seconds. The response is plotted in terms of a scaled wavenumber $m\Delta\lambda/\pi$. For these parameter values, the case of zero physical response mentioned earlier occurs at $m\Delta\lambda/\pi \approx 0.07$ and this is seen by the jumps near this value.

For an exact solution we would have the response equal to 1, indicated by the dotted line in each plot. For $\Delta t = 600$s (solid line) we get acceptable results. At the longer timestep of $\Delta t = 3600$s (dashed) there is clearly a resonant response when $m\Delta\lambda/\pi \approx 0.56$. This is the first resonance given by (19), when $\theta = \frac{\pi}{2}$.

4.3. *Linear analysis: SLLT*

We now turn to the SLLT scheme to examine its effect on orographically forced waves. Taking the Laplace transform of each equation along a trajectory, as discussed in §2.2, and again looking for steady state spherical harmonic solutions of the form (15), we get

$$\begin{aligned} s\widehat{\zeta} - \zeta_D^n + f\widehat{\delta} &= 0 \\ s\widehat{\delta} - \delta_D^n - f\widehat{\zeta} - \frac{\ell(\ell+1)}{a^2}\widehat{\Phi} &= 0 \\ s\widehat{\Phi} - \Phi_D^n + \bar{\Phi}\widehat{\delta} &= s\widehat{\Phi_s} - (\Phi_s)_D^n \end{aligned}$$

Considering the trajectory $\lambda = \lambda_D + \bar{\omega}t$, we can write

$$\begin{aligned} \widehat{\Phi}_s &\equiv \mathfrak{L}\left\{(\Phi_s)_\ell^m\; e^{im(\lambda_D + \bar{\omega}t)}\, P_\ell^m(\mu)\right\} \\ &= (\Phi_s)_D^n\;\; \mathfrak{L}\left\{e^{im\bar{\omega}t}\right\} \end{aligned}$$

We must consider the transform of $e^{im\bar{\omega}t}$. This is a function of time only, since $\bar{\omega}$ is a constant with no spatial variation. Therefore we can write $\mathfrak{L}\left\{e^{im\bar{\omega}t}\right\} = \frac{1}{s - im\bar{\omega}}$. Using this we can write the transformed system as

$$\mathbf{M}\,\widehat{\mathbf{X}} = \mathbf{X}_D^n + \mathbf{R}_s \qquad (20)$$

where $\mathbf{X} = (\zeta, \delta, \Phi)^T$,

$$\mathbf{M} = \begin{pmatrix} s & f & 0 \\ -f & s & -\dfrac{\ell(\ell+1)}{a^2} \\ 0 & \bar{\Phi} & s \end{pmatrix}$$

and

$$\mathbf{R}_s = \begin{pmatrix} 0 \\ 0 \\ \dfrac{i\,m\,\bar{\omega}}{s - i\,m\,\bar{\omega}}\,(\Phi_s)_D^n \end{pmatrix}$$

The right-hand side has been split so as to isolate the response due to the orographic term. We focus first on this response; that is, we consider the system

$$\mathbf{M}\,\widehat{\mathbf{X}}_{\rm orog} = \mathbf{R}_s$$

Solving for $(\widehat{\Phi})_{\rm orog}$ we get

$$(\widehat{\Phi})_{\rm orog} = i\,m\,\bar{\omega}\;(\Phi_s)_D^n\;\frac{s^2 + f^2}{s\,(s^2 + G_\ell^2)\,(s - i\,m\,\bar{\omega})}$$

We see immediately that we cannot have $s = 0$, $s = i\,m\,\bar{\omega}$ or $s = \pm iG_\ell$. But $|s| = \gamma$, the radius of the inversion contour and so these situations can be avoided by a careful contour choice.

The operator $\mathfrak{L}_N^*$ is applied to $(\widehat{\Phi})_{\rm orog}$ to recover the physical field. The expression for $(\widehat{\Phi})_{\rm orog}$ can first be expanded using partial fractions. We can then apply $\mathfrak{L}_N^*$ and use the following results from Part 1 of this work:

$$\mathfrak{L}_N^*\left\{\frac{1}{s - i\,\nu}\right\} = H_N(\nu)\, e_N^{i\,\nu\,\Delta t} \quad \text{and} \quad \mathfrak{L}_N^*\left\{\frac{1}{s}\right\} = 1$$

These results give us the physical solution obtained when we apply the numerical inversion operator to each term in $(\widehat{\Phi})_{\rm orog}$. After inverting we get

$$(\Phi_{\rm orog})_A = R'\;(\Phi_s)_D^n \qquad (21)$$

where

$$\begin{aligned} R' = {} & \frac{f^2 - (m\,\bar{\omega})^2}{G_\ell^2 - (m\,\bar{\omega})^2}\, H^+(m\,\bar{\omega}) - \left(\frac{f}{G_\ell}\right)^2 \\ & + \frac{m\,\bar{\omega}\,\mathcal{F}}{2\,(G_\ell - m\,\bar{\omega})}\, H^+(G_\ell) - \frac{m\,\bar{\omega}\,\mathcal{F}}{2\,(G_\ell + m\,\bar{\omega})}\, H^-(G_\ell) \end{aligned}$$

with

$$H^\pm(x) = H_N(x)\, e_N^{\pm\, i\,x\,\Delta t} \quad \text{and} \quad \mathcal{F} = 1 - \left(\frac{f}{G_\ell}\right)^2$$

Since

$$\begin{aligned} (\Phi_s)_D &= (\Phi_s)_\ell^m\, e^{i\,m\,\lambda_D}\, P_\ell^m(\mu) \\ &= (\Phi_s)_\ell^m\, e^{i\,m\,\lambda_A}\, e^{-i\,2\theta}\, P_\ell^m(\mu) \end{aligned}$$

we can divide (21) by $e^{i\,m\,\lambda_A}\,P_\ell^m(\mu)$ and write $(\Phi_{\rm orog})_\ell^m = e^{-i\,2\,\theta} R'\,(\Phi_s)_\ell^m$.

We now note that the full solution of (11) is composed of a free component and a forced response. To ensure that the solution of (20) agrees with the physical one in the limit $\bar{\omega} = 0$ (see (13)), we choose the initial condition

$$\Phi_{\rm geo} = \frac{f^2}{G_\ell^2}\,\Phi_s$$

with vanishing divergence and geostrophic vorticity. For this steady flow we have $(\Phi_{\rm geo})_A = (\Phi_{\rm geo})_D$ and, similar to the analysis in the previous paragraph, we can write $(\Phi_{\rm geo})_\ell^m = e^{-i\,2\,\theta}\,\frac{f^2}{G_\ell^2}\,(\Phi_s)_\ell^m$. Now the total solution satisfies

$$\Phi_\ell^m = \left\{\frac{f^2}{G_\ell^2} + R'\right\} e^{-i\,2\,\theta}\,(\Phi_s)_\ell^m$$

As in the SLSI case, we divide the numerical response by the analytic response (13) to get

$$\begin{aligned} R_{\rm SLLT} &= H^+(m\bar{\omega})\,e^{-i\,2\,\theta} \\ &+ e^{-i\,2\,\theta}\,H_N(G_\ell)\,\frac{m\,\bar{\omega}\,\left(1-\left(\frac{f}{G_\ell}\right)^2\right)}{f^2-(m\,\bar{\omega})^2}\times \\ &\{m\bar{\omega}\,\cos_N(G_\ell\Delta t) + i\,G_\ell\,\sin_N(G_\ell\Delta t)\} \end{aligned} \qquad (22)$$

where $\cos_N(x)$ and $\sin_N(x)$ denote, respectively, the real and imaginary parts of e_N^{ix}. The response in (22) will only have a zero denominator for $f^2 = (m\bar{\omega})^2$. This is, however, the case of zero physical response as mentioned in the SLSI analysis. Thus we expect *no spurious resonant response to orography* using a SLLT discretisation.

To illustrate this, we plot $R_{\rm SLLT}$ in the right-hand panel of Figure 3 with parameters matching those for SLSI. In addition we use the values $N = 8$ and $\tau_c = 6$ hours. For SLLT, however, there is no resonant behaviour present.

On comparison with the SLSI resonances on the left in Figure 3, it may appear that we are resonance-free simply because the problematic wavenumbers have been removed by the LT filtering. However, it is important to note again that the expression in (22) shows no artificial resonance, regardless of wavenumber. To demonstrate this we plot $R_{\rm SLSI}$ and $R_{\rm SLLT}$ in Figure 4, this time for T213 resolution and a 2 hour timestep. For the SLLT discretisation we choose a less severe cutoff of 3 hours and $N = 16$. With these parameter values we see resonant behaviour in SLSI around $m\Delta\lambda/\pi$ between 0.1 and 0.2. The SLLT plot to the right of this show that these scales are being retained, but with no resonance.

4.4. Shallow water experiments

We now move to numerical tests with the fully nonlinear shallow water system, using the SLSI and SLLT models. A number of previous authors have used the analysis at 12 UTC on the 12th of February 1979 as a case study [Rivest et al. (1994), Rivest and Staniforth (1995), Li and Bates (1996), Ritchie and Tanguay (1996)]. There is a strong flow over the Rocky mountains, so this is very suitable for investigating orographic resonance

The initial conditions are the 500hPa winds and geopotential height, as well as the surface geopotential, taken from the ERA-40 dataset of the ECMWF (Uppala et al., 2005). We initialise with the Laplace transform initialsation method, as outlined in Part 1.

The simulations to be presented were all run at a T119 resolution with no added diffusion. The SLLT parameters used were $N = 8$ and $\tau_c = 6$ hours. As predicted by the linear analysis, forecasts using a 600 second timestep did not suffer from any spurious orographic resonance, since this only becomes an issue at high CFL numbers. We focus on the North American continent and show the 24-hour forecasted height using a one hour timestep. The linear analysis suggests that we may encounter problems with orographic resonance for the longer timestep. In Figure 5 we plot the height at 24 hours using the SLSI (left) and SLLT (right) models. The SLSI model shows very pronounced noise over the mountains. As expected from the linear analysis, the SLLT model does not suffer from this resonance.

4.5. SETTLS Formulation

When discretising the shallow water equations (1) for SLSI and SLLT, we evaluated the nonlinear terms at the midpoint of the trajectory. A number of alternative treatments of the nonlinear terms have been proposed. As mentioned, Tanguay et al. (1992) recommend a spatial averaging, which helps to alleviate orographic noise and also reduces the number of interpolations necessary. Gospodinov et al. (2001) discuss how this has been shown to lead to problems, with non-meteorological noise being observed in a number of forecasting centres. This was solved at ECMWF with the operational introduction of the 'Stable Extrapolation Two-Time-Level Scheme', or SETTLS (Hortal, 2002). Durran and Reinecke (2004) show that, out of the class of schemes studied by Gospodinov et al., optimal stability is obtained with SETTLS.

The transform of a general prognostic equation was given by (7), where the nonlinear terms were evaluated at the trajectory midpoint as $N_M^{n+\frac{1}{2}}$. The SETTLS scheme evaluates the nonlinear terms using $\frac{1}{2}\left\{\left(2\,N_D^n - N_D^{n-1}\right) + N_A^n\right\}$. We incorporated this into SLSI. Everything else in the models, including the trajectory calculations, was unchanged. When tested with the cases used in §3, SETTLS version of SLSI showed improved accuracy over the original (see Clancy (2010) for further details).

For the orographic resonance test case, we plot the 24 hour forecast height using SLSI SETTLS with a one hour timestep in Figure 6. Comparing with Figure 5, we see the SETTLS treatment greatly reduces the distortions over the mountains, but nevertheless it is still present. The SLLT discretisation is still the most effective for removing the spurious response.

5. Conclusion

We have developed a semi-Lagrangian shallow water model using the Laplace transform filtering integration method. This permits forecasts with longer timesteps than could be used for an Eulerian model and compares favourably with a reference semi-Lagrangian semi-implicit (SLSI) scheme in terms of accuracy. We investigated the problem of

orographic resonance associated with SLSI discretisations. By means of a linear analysis and also shallow water simulations, the SLLT model was shown to be free from this spurious noise.

The Laplace transform integration method has been tested in a shallow water model. Its advantages should also hold for baroclinic models used in operational NWP. Its capacity to filter high-frequency waves should be of particular benefit in the context of nonhydrostatic models.

Acknowledgements

The authors are grateful to John Drake for providing the Matlab shallow water code, to Eigil Kaas for originally suggesting the use of the LT method in the context of orographic resonance, and to the reviewers for their helpful comments. This research was funded by the Irish Research Council for Science, Engineering and Technology Post-Graduate Scholarship Scheme and a UCD Research Demonstratorship.

References

Bates JR, McDonald A. 1982. Multiply-Upstream, Semi-Lagrangian Advective Schemes: Analysis and Application to a Multi-Level Primitive Equation Model. *Mon. Weather Rev.* **110**: 1831–1842

Caya D, Laprise R. 1999. A Semi-Implicit Semi-Lagrangian Regional Climate Model: The Canadian RCM. *Mon. Weather Rev.* **127**: 341–362

Clancy C. 2010. *A Laplace Transform Filtering Integration Scheme for Numerical Weather Prediction.* PhD Thesis, University College Dublin (Sept. 2010) `http://mathsci.ucd.ie/~plynch/candl.html`.

Clancy C, Lynch P. 2011. Laplace transform integration of the shallow water equations. Part 1: Eulerian formulation and Kelvin waves. Submitted to *Q. J. R. Meteorol. Soc.*

Coiffier J, Chapelet P, Marie N. 1987. 'Study of various quasi-Lagrangian techniques for numerical models', In *Proceedings of ECMWF Workshop on Techniques for Horizontal Discretization in Numerical Weather Prediction Models*, 19–46. ECMWF, Reading, UK

Côté J, Gravel S, Staniforth A. 1995. A Generalized Family of Schemes that Eliminate the Spurious Resonant Response of Semi-Lagrangian Schemes to Orographic Forcing. *Mon. Weather Rev.* **123**: 3605–3613

Côté J, Staniforth A. 1988. A Two-Time-Level Semi-Lagrangian Semi-implicit Scheme for Spectral Models. *Mon. Weather Rev.* **116**: 2003–2012

Drake JB, Guo DX. 2001. *'A vorticity-divergence global semi-Lagrangian spectral model for the shallow water equations'*. Technical Report ORNL/TM-2001/216: Oak Ridge National Laboratory, Tennessee

Drake JB, Worley P, D'Azevedo E. 2008. Algorithm 888: Spherical Harmonic Transform Algorithms. *ACM Trans. Math. Software* **35**. No. 3. Article 23

Durran DR. 1999. *Numerical Methods for Wave Equations in Geophysical Fluid Dynamics*, Springer

Durran DR, Reinecke PA. 2004. Instability in a class of explicit two-time-level semi-Lagrangian schemes. *Q. J. R. Meteorol. Soc.* **130**: 365–369

Gospodinov IG, Spiridonov VG, Geleyn J-F. 2001. Second-order accuracy of two-time-level semi-Lagrangian schemes. *Q. J. R. Meteorol. Soc.* **127**: 1017–1033

Héreil P, Laprise R. 1996. Sensitivity of Internal Gravity Waves Solutions to the Time Step of a Semi-Implicit Semi-Lagrangian Nonhydrostatic Model. *Mon. Weather Rev.* **124**: 972–999

Hortal M. 2002. The development and testing of a new two-time-level semi-Lagrangian scheme (SETTLS) in the ECMWF forecast model. *Q. J. R. Meteorol. Soc.* **128**: 1671–1687

Li Y, Bates JR. 1996. A study of the behaviour of semi-Lagrangian models in the presence of orography. *Q. J. R. Meteorol. Soc.* **122**: 1675–1700

Lindberg K, Alexeev VA. 2000. A Study of the Spurious Orographic Resonance in Semi-Implicit Semi-Lagrangian Models. *Mon. Weather Rev.* **128**: 1982–1989

Lynch P. 1991. Filtering Integration Schemes Based on the Laplace and Z Transforms. *Mon. Weather Rev.* **119**: 653–666

Ritchie H, Beaudoin C. 1994. Approximations and Sensitivity Experiments with a Baroclinic Semi-Lagrangian Spectral Model. *Mon. Weather Rev.* **122**: 2391–2399

Ritchie H, Tanguay M. 1996. A Comparison of Spatially Averaged Eulerian and Semi-Lagrangian Treatments of Mountains. *Mon. Weather Rev.* **124**: 167–181

Rivest C, Staniforth A. 1995. Modifying the Conventional Three-time-level Semi-implicit Semi-Lagrangian Scheme to Eliminate Orographically Induced Spurious Resonance. *Atmospheric-Ocean* **33**: 109–119

Rivest C, Staniforth A, Robert A. 1994. Spurious Resonant Response of Semi-Lagrangian Discretizations to Orographic Forcing: Diagnosis and Solution. *Mon. Weather Rev.* **122**: 366–376

Robert A. 1981. A Stable Numerical Integration Scheme for the Primitive Meteorological Equations. *Atmosphere-Ocean* **19**: 35–46

Robert A. 1982. A Semi-Lagrangian and Semi-Implicit Numerical Integration Scheme for the Primitive Meteorological Equations. *J. Meteorol. Soc. Japan* **60**: 319–325

Staniforth A, Côté J. 1991. Semi-Lagrangian Integration Schemes for Atmospheric Models - A Review. *Mon. Weather Rev.* **119**: 2206–2223

Tanguay M, Yakimiw E, Ritchie H, Robert A. 1992. Advantages of Spatial Averaging in Semi-implicit Semi-Lagrangian Schemes. *Mon. Weather Rev.* **120**: 113–123

Temperton C, Horal M, Simmons A. 2001. A two-time-level semi-Lagrangian global spectral model. *Q. J. R. Meteorol. Soc.* **127**: 111–127

Temperton C, Staniforth A. 1987. An efficient two-time-level semi-Lagrangian semi-implicit integration scheme. *Q. J. R. Meteorol. Soc.* **113**: 1025–1039

Uppala SM, Kållberg PW, Simmons AJ, Andrae U, Da Costa Bechtold V, Fiorino M, Gibson JK, Haseler J, Hernandez A, Kelly GA, Li X, Onogi K, Saarinen S, Sokka N, Allan RP, Andersson E, Arpe K, Balmaseda MA, Geljaars ACM, Van De Berg L, Bidlot J, Bormann N, Caires S, Chevallier F, Dethof A, Dragosavac M, Fisher M, Fuentes M, Hagemann S, Hólm E, Hoskins BJ, Isaksen L, Janssen PAEM, Jenne R, McNally AP, Mahfouf J-F, Morcrette J-J, Rayner NA, Saunders RW, Simon P, Sterl A, Trenberth KE, Untch A, Vasiljevic D, Viterbo P, Woollen J. 2005. The ERA-40 re-analysis. *Q. J. R. Meteorol. Soc.* **131**: 2961–3012

Williamson DL, Drake JB, Hack JJ, Jakob R, Swarztrauber PN. 1992. A Standard Test Set for Numerical Approximation to the Shallow Water Equations in Spherical Geometry. *J. Comp. Phys.* **102**: 211–224

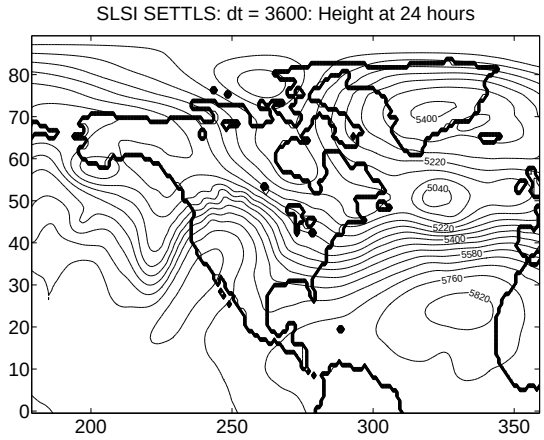

Figure 6. 24-hour height forecasts at $\Delta t = 3600$s for SLSI SETTLS

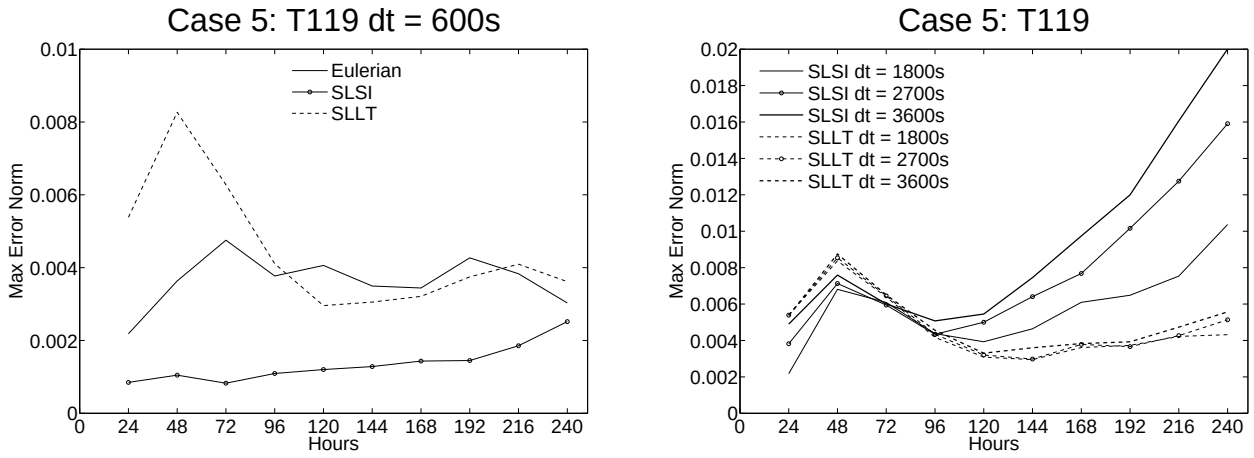

Figure 1. l_∞ errors for Case 5 for various timesteps

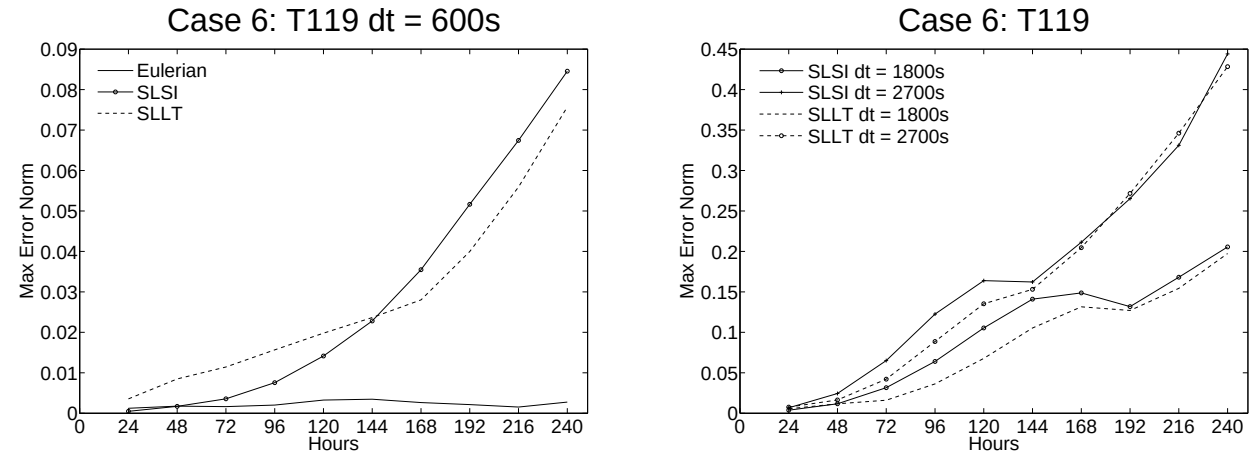

Figure 2. l_∞ errors for Case 6 for various timesteps

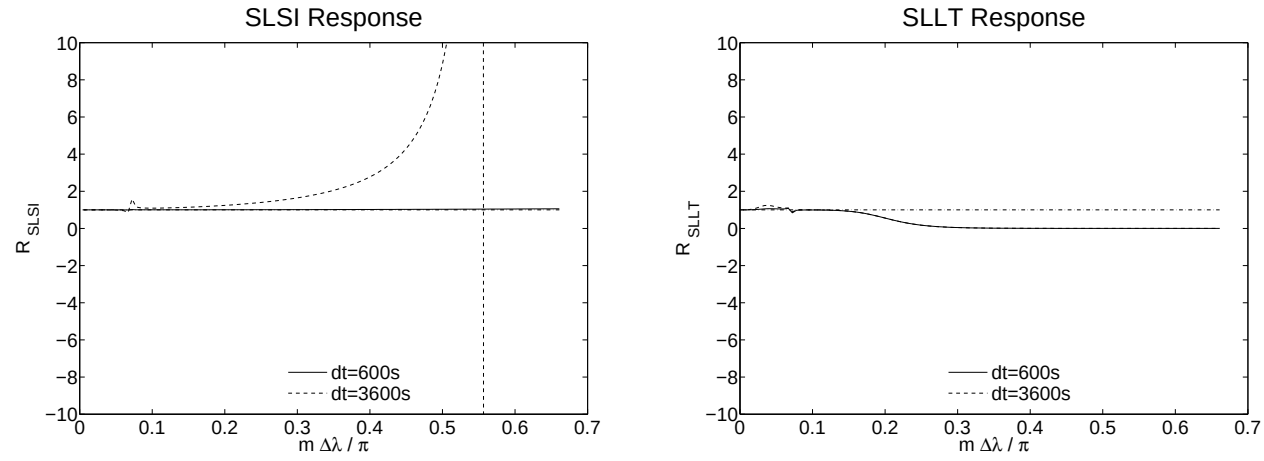

Figure 3. Numerical response to orographic forcing divided by the physical response. The dash-dot line is $R = 1$, where the numerical solution equals the analytic solution. Left: SLSI. Right: SLLT. Note that the extremes at $m\Delta\lambda/\pi \approx 0.07$ are artefacts, due to the vanishing of the physical solution.

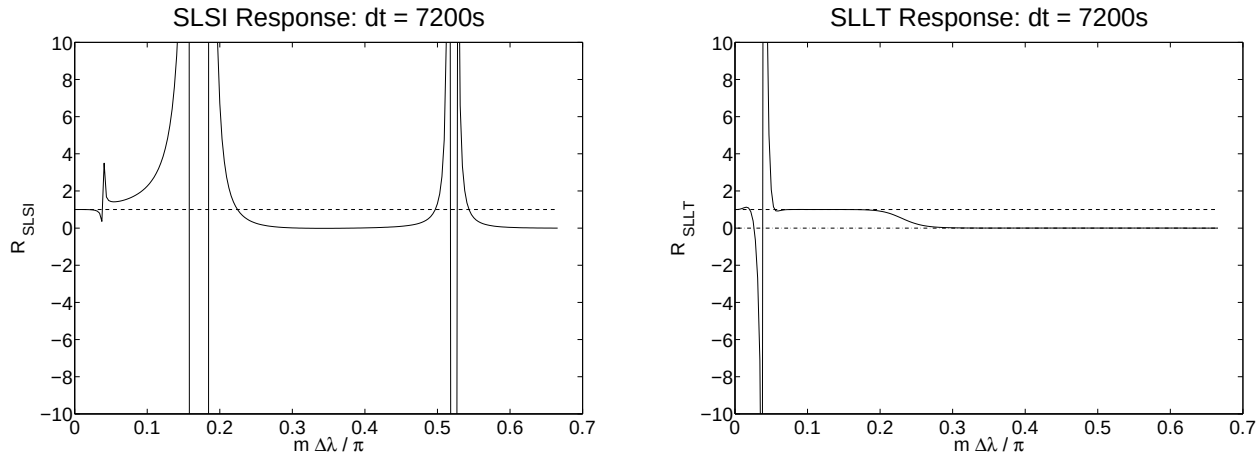

Figure 4. Responses for SLSI and SLLT, T213 with $\Delta t = 7200$s, $N = 16$ and $\tau_c = 3$ hours: the numerical response to orographic forcing divided by the physical response. The dashed line is $R = 1$, where the numerical solution equals the analytic solution and the dot-dashed line is $R = 0$, where the numerical solution is zero due to filtering. The extremes at $m\Delta\lambda/\pi \approx 0.04$ are artefacts, due to the vanishing of the physical solution.

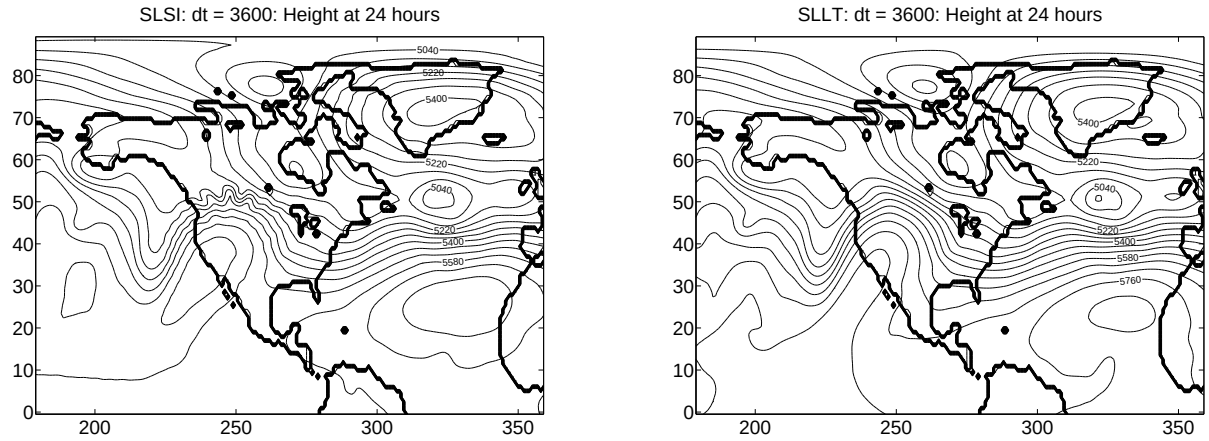

Figure 5. 24-hour height forecasts at $\Delta t = 3600$s for SLSI (left) and SLLT (right)